Article

In Situ Single-Crystal X-ray Diffraction Studies of Desorption and Sorption in a Flexible Nanoporous Molecular Framework Material

Gregory J. Halder, and Cameron J. Kepert

J. Am. Chem. Soc., **2005**, 127 (21), 7891-7900• DOI: 10.1021/ja042420k • Publication Date (Web): 05 May 2005

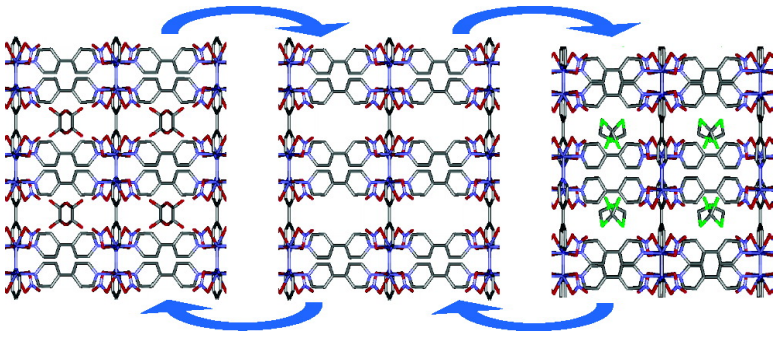

J|A|C|S
ARTICLES
Published on Web 05/05/2005

In Situ Single-Crystal X-ray Diffraction Studies of Desorption and Sorption in a Flexible Nanoporous Molecular Framework Material

Gregory J. Halder and Cameron J. Kepert*

Contribution from the School of Chemistry, University of Sydney, NSW 2006, Australia

Received December 17, 2004; E-mail: c.kepert@chem.usyd.edu.au

Abstract: The subtle flexibility of the framework material $Co(bpy)_{1.5}(NO_3)_2$·(guest) (bpy = 4,4′-bipyridine) (**1·(guest)**) is demonstrated quantitatively through in situ single-crystal X-ray diffraction measurements of guest desorption and sorption processes. Variable temperature unit cell determinations were employed to monitor the uptake and release of guest species, and full structural determinations have been carried out for the as-grown ethanol-loaded framework (**1·(EtOH)**), for the empty host framework (**1**), and for each of the five introduced guests (methanol: **1·(MeOH)**, acetone: **1·(ACN)**, acetonitrile: **1·(MeCN)**, tetrahydrofuran: **1·(THF)**, dichloromethane: **1·(DCM)**). The framework consists of interdigitated two-dimensional bilayers of cobalt(II) centers bridged by bpy ligands, with one-dimensional pores that account for approximately 20% of the total volume. The sorption of guest species of varying size and shape has revealed the framework's ability to adapt to different guests through a range of different framework flexibilities.

Introduction

The potential for porous metal−organic framework materials to mimic many of the host−guest properties of commercially important porous materials (e.g., zeolites)[1] and to expand into novel areas such as molecular sensing,[2] gas storage,[3−6] and chiral separations[7−9] is now widely recognized. A key step in investigating this potential involves the development of suitable techniques for monitoring guest exchange in this relatively new class of materials. Consequently, guest-exchange studies have become more predominant in this area, with a recent review tabulating more than 50 examples.[10] These studies typically rely on the measurement of gas and vapor isotherms,[11−13] thermogravimetric analysis, and powder diffraction[6,14] to monitor the uptake and release of guest molecules, although NMR, gas chromatography, and vibrational spectroscopic studies have also been reported.[6,10,15] Recently, single-crystal X-ray diffraction investigations of empty and guest-loaded materials that retain their monocrystallinity during ex situ desorption and sorption processes have produced a wealth of information on the flexible nature of coordination framework hosts.[5,9,16−20]

Here we pioneer a novel in situ single-crystal X-ray diffraction technique to follow, as a function of temperature and vapor pressure, the sorption and desorption of different guest species into a porous coordination framework. This technique allows continuous monitoring of the single-crystal structure during guest desorption and sorption. The work builds on our earlier

(1) (a) Kitagawa, S.; Kitaura, R.; Noro, S.-I. *Angew. Chem., Int. Ed.* **2004**, *43*, 2334−2375. (b) Yaghi, O. M.; O'Keeffe, M.; Ockwig, N. W.; Chae, H. K.; Eddaoudi, M.; Kim, J. *Nature* **2003**, *423*, 705−714. (c) Janiak, C. *J. Chem. Soc., Dalton Trans.* **2003**, 2781−2804. (d) Rosseinsky, M. J. *Microporous Mesoporous Mater.* **2004**, *73*, 15−30. (e) Soldatov, D. V. *J. Inclusion Phenom. Macrocyclic Chem.* **2004**, *48*, 3−9.
(2) (a) Halder, G. J.; Kepert, C. J.; Moubaraki, B.; Murray, K. S.; Cashion, J. D. *Science* **2002**, *298*, 1762−1765. (b) Real, J. A.; Andres, E.; Muñoz, M. C.; Julve, M.; Granier, T.; Bousseksou, A.; Varret, F. *Science* **1995**, *268*, 265−267.
(3) Rowsell, J. L. C.; Millward, A. R.; Park, K. S.; Yaghi, O. M. *J. Am. Chem. Soc.* **2004**, *126*, 5666−5667.
(4) Zhao, X. B.; Xiao, B.; Fletcher, A. J.; Thomas, K. M.; Bradshaw, D.; Rosseinsky, M. J. *Science* **2004**, *306*, 1012−1015.
(5) Eddaoudi, M.; Kim, J.; Rosi, N. L.; Vodak, D.; Wachter, J.; O'Keeffe, M.; Yaghi, O. M. *Science* **2002**, *295*, 469−472.
(6) Kitaura, R.; Kitagawa, S.; Kubota, Y.; Kobayashi, T. C.; Kindo, K.; Mita, Y.; Matsuo, A.; Kobayashi, M.; Chang, H.-C.; Ozawa, T. C.; Suzuki, M.; Sakata, M.; Takata, M. *Science* **2002**, *298*, 2358−2361.
(7) (a) Bradshaw, D.; Prior, T. J.; Cussen, E. J.; Claridge, J. B.; Rosseinsky, M. J. *J. Am. Chem. Soc.* **2004**, *126*, 6106−6114. (b) Seo, J. S.; Whang, D.; Lee, H.; Jun, S. I.; Oh, J.; Jeon, Y. J.; Kim, K. *Nature* **2000**, *404*, 982−986.
(8) Kepert, C. J.; Prior, T. J.; Rosseinsky, M. J. *J. Am. Chem. Soc.* **2000**, *122*, 5158−5168.
(9) Abrahams, B. F.; Jackson, P. A.; Robson, R. *Angew. Chem., Int. Ed.* **1998**, *37*, 2656−2659.
(10) James, S. L. *Chem. Soc. Rev.* **2003**, *32*, 276−288.
(11) Eddaoudi, M.; Li, H.; Yaghi, O. M. *J. Am. Chem. Soc.* **2000**, *122*, 1391−1397.
(12) Kondo, M.; Yoshitomi, T.; Seki, K.; Matsuzaka, H.; Kitagawa, S. *Angew. Chem., Int. Ed. Engl.* **1997**, *36*, 1725−1727.
(13) Fletcher, A. J.; Cussen, E. J.; Prior, T. J.; Rosseinsky, M. J.; Kepert, C. J.; Thomas, K. M. *J. Am. Chem. Soc.* **2001**, *123*, 10001−10011.
(14) Matsuda, R.; Kitaura, R.; Kitagawa, S.; Kubota, Y.; Kobayashi, T. C.; Horike, S.; Takata, M. *J. Am. Chem. Soc.* **2004**, *126*, 14063−14070.
(15) (a) Nossov, A. V.; Soldatov, D. V.; Ripmeester, J. A. *J. Am. Chem. Soc.* **2001**, *123*, 3563−3568. (b) Uemura, K.; Kitagawa, S.; Fukui, K.; Saito, K. *J. Am. Chem. Soc.* **2004**, *126*, 3817−3828.
(16) (a) Li, H.; Eddaoudi, M.; O'Keeffe, M.; Yaghi, O. M. *Nature* **1999**, *402*, 276−279. (b) Abrahams, B. F.; Moylan, M.; Orchard, S. D.; Robson, R. *Angew. Chem., Int. Ed.* **2003**, *42*, 1848−1851. (c) Rather, B.; Zaworotko, M. J. *Chem. Commun.* **2003**, 830−831. (d) Ganesan, P. V.; Kepert, C. J. *Chem. Commun.* **2004**, 2168−2169.
(17) (a) Biradha, K.; Hongo, Y.; Fujita, M. *Angew. Chem., Int. Ed.* **2000**, *39*, 3843−3845. (b) Choi, E. Y.; Kim, Y.; Seff, K. *J. Phys. Chem. B* **2002**, *106*, 5827−5832. (c) Kurmoo, M.; Kumagai, H.; Hughes, S. M.; Kepert, C. J. *Inorg. Chem.* **2003**, *42*, 6709−6722. (d) Lee, E. Y.; Suh, M. P. *Angew. Chem., Int. Ed.* **2004**, *43*, 2798−2801. (e) Suh, M. P.; Ko, J. W.; Choi, H. J. *J. Am. Chem. Soc.* **2002**, *124*, 10976−10977. (f) Soldatov, D. V.; Enright, G. D.; Ripmeester, J. A. *Cryst. Growth Des.* **2004**, *4*, 1185−1194.
(18) (a) Biradha, K.; Fujita, M. *Angew. Chem., Int. Ed.* **2002**, *41*, 3392−3395. (b) Ohmori, O.; Kawano, M.; Fujita, M. *J. Am. Chem. Soc.* **2004**, *126*, 16292−16293.
(19) Biradha, K.; Hongo, Y.; Fujita, M. *Angew. Chem., Int. Ed.* **2002**, *41*, 3395−3398.
(20) Choi, H. J.; Suh, M. P. *J. Am. Chem. Soc.* **2004**, *126*, 15844−15851.

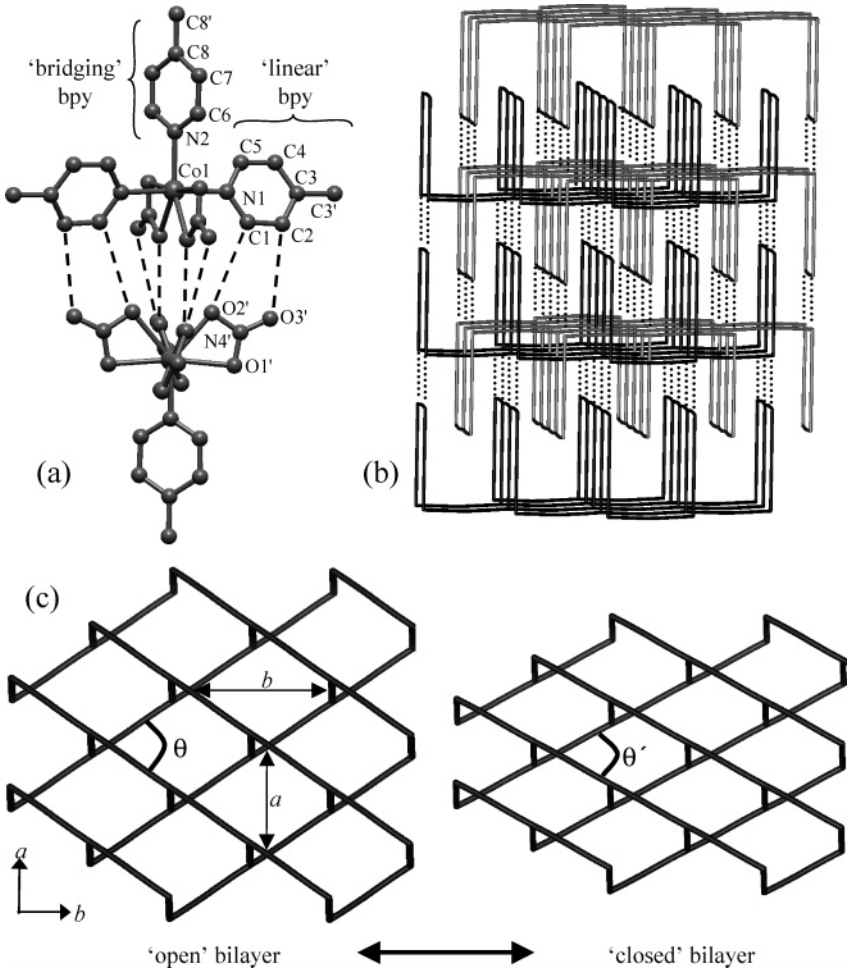

Figure 1. Structural motif of **1**: (a) Ball-and-stick representation of the T-shaped coordination of bpy about Co showing the labeling of all atoms in the asymmetric unit. Hydrogen atoms are omitted for clarity. Eight hydrogen bonds form between the aromatic C−H groups and oxygen atoms from nitrate anions. (b) Stick representation of the interdigitation of bilayers illustrating the hydrogen bonding between alternate bilayers that impart a 3-D nature to the framework structure. The sticks represent linear Co(bpy) strands along the *ab* plane connected into bilayers along *c* by bpy groups. Alternate bilayers are colored gray and black for clarity. Each dashed line represents eight C−H···O interactions. (c) Stick representation of individual bilayer illustrating the "garden-trellis" action and the bilayer torsion angle, θ. θ can be readily calculated from the *a* and *b* unit cell parameters that define the bilayer dimensions, $\theta = 2(\arctan(a/b))$.

use of in situ single-crystal diffraction to follow guest desorption from the extremely robust coordination framework $Ni(bpy)_{1.5}(NO_3)_2 \cdot (EtOH)$.[21] This involved the collection of variable temperature unit cell determinations to monitor the single-crystal desolvation process, followed by a full structural determination of the empty host framework. The aim here has been to extend this technique to monitor the sorption and desorption of new guests within this remarkably stable host.

The $M(bpy)_{1.5}(NO_3)_2 \cdot (guest)$ (M = Co, Ni, or Zn) framework is formed by the assembly of chiral bilayers of opposite handedness into a tongue-and-groove-type structure. Each bilayer results from the T-shaped coordination around the metal center of three bpy units, with two nitrate anions completing the coordination sphere (Figure 1a). There are two crystallographically independent bpy units distinguished as either "linear" or "bridging". One links the metal centers to form parallel linear chains in the *ab* plane ("linear"), and the other bridges neighboring chains along *z* ("bridging"). The presence of C−H···O hydrogen bonds between the nitrate anions and the bpy groups of alternate bilayers imparts a *pseudo*-three-dimensional topology, which may be considered as the interpenetration of two semi-regular $6^4(6,10)^1$-type three-dimensional networks (Figure 1b).[22]

The interdigitation of the bilayers defines one-dimensional channels parallel to the *a*-axis of approximately 6×3 Å^2. In the as-grown Ni(II) analogue, these channels are occupied by ethanol molecules that form hydrogen bonds with neighboring nitrate groups. The guests are liberated slowly at room temperature and can be completely removed with heating to 100 °C. The empty framework material, $Ni(bpy)_{1.5}(NO_3)_2$, is then stable to 230 °C.[21] The robust nature of the framework is reflected in the retention of a small crystal mosaicity upon desolvation. Remarkably, guest loss does not involve symmetry change or channel volume collapse, but only a slight relaxation due primarily to a subtle scissor-like action of the bilayers. This action is illustrated in Figure 1c and can be quantified by the bilayer torsion angle, θ.

The adsorption dynamics of a range of gases and vapors for the $Ni(bpy)_{1.5}(NO_3)_2$ framework have been reported.[4,12,13,23,24] Notably, a highly detailed analysis of the adsorption charac-

(21) Kepert, C. J.; Rosseinsky, M. J. *Chem. Commun.* **1999**, 375−376.

(22) Wells, A. F. *Three Dimensional Nets and Polyhedra*; Wiley: New York, 1977.

teristics of nitrogen, argon, carbon dioxide, nitrous oxide, ethanol, and methanol gases and vapors has been performed over a range of temperatures as a function of pressure.[13,23] The results were surprisingly complex, with steps occurring in the isotherms dependent on both the guest and the temperature. The porous framework was found to be flexible with host−guest interactions modifying the pore windows that form a barrier to diffusion. This work provided novel evidence of specific host−guest interactions leading to structural change in flexible porous framework materials. The present structural studies were employed to characterize these interactions and structural changes.

Here we extend our use of the in situ single-crystal X-ray diffraction technique on this phase[21] to investigate the structural consequences of the sorption and desorption of new guest species into the cobalt(II) analogue. In the cobalt(II) phases, **1·(guest)**, the nitrate ligands exhibit a symmetric mode of binding that, in turn, simplifies the crystallography; both nitrate ligands are bidentate in **1·(guest)** compared to one bidentate and one monodentate for the nickel(II) analogue. In total, the sorption of five new guests has been fully characterized by single-crystal X-ray diffraction, yielding considerable insight into the ability of the host lattice to adapt to guests of different shapes, sizes, and chemical properties. In each case, the in situ monitoring of guest sorption demonstrates that this process occurs uniformly over the single-crystal samples, there being no observed increase in the crystal mosaicities and no evidence for partial ordering of guests in the channels.

Experimental Section

Synthetic Method. 1·(EtOH) was prepared by diffusion of bpy (100 mg, 0.64 mmol) and cobalt(II) nitrate (124 mg, 0.43 mmol) through ethanol in an H-shaped tube (60 mL). Purple crystals of **1·(EtOH)** grew over a period of 1 month.

Thermogravimetry. Measurements were carried out on a TA Instruments Hi-Res TGA 2950 thermogravimetric analyzer. The atmosphere was controlled with a sorptive-filled bubbler with a gas bypass attached to a dry dinitrogen supply (0.1 L·min^{-1}), allowing either a dry dinitrogen or a sorptive vapor/dinitrogen stream to flow through the system. The sorptive reservoir of the bubbler was placed in an ice bath (0 °C) to prevent condensation inside the analyzer (vapor pressures for guest solvents at 0 °C (kPa): MeOH 4.03, EtOH 1.50, ACN 9.35, MeCN 17.7, THF 7, DCM 19.2). To identify the approximate temperature of guest loss and thermal decomposition, the temperature was ramped at 2 °C·min^{-1} from 20 to 500 °C under a dry dinitrogen atmosphere. For sorption measurements the sample temperature was ramped at 0.5 °C·min^{-1} to approximately 110 °C and held for 1 h under a dinitrogen atmosphere. The bubbler was then switched to supply sorptive vapor to the system for the remainder of the experiment. The temperature was maintained for an additional 1 h before cooling at 0.5 °C·min^{-1} to 25 °C and remained at this temperature for 6 h. Figures for all TGA data are included in the Supporting Information.

Single-Crystal X-ray Diffraction − Structural Refinements. Diffraction data were collected on a Bruker Smart 1000 CCD equipped with Mo Kα ($\lambda = 0.71073$ Å) radiation and Oxford Instruments nitrogen gas cryostream. Crystals of **1·(EtOH)** were mounted with a thin smear of grease in an open-ended glass capillary to allow the guest ethanol molecules to be liberated as the temperature was ramped to 375 K (20 K·h^{-1}). To ensure complete desolvation, this temperature was maintained until no further changes in the unit cell parameters were observed. For resolvation, a small wad of dried cotton wool moistened with several drops of the desired guest solvent (doubly distilled over suitable desiccant) was placed in the end of the capillary such that there was an air space between the cotton wool and the crystal. The capillary was then sealed with a greased Teflon cap, allowing solvation to occur only in the vapor phase. The crystals were cooled (10−15 K·h^{-1}) to near ambient temperatures, the final temperature depending on the nature of the sorptive with the need to prevent solvent condensation on the crystal (see Results section for temperatures). To confirm reversibility, the cap was then removed from the capillary and the desolvation process was repeated as described above. Full spheres of data were collected over a range of incident angles, up to 2000 0.3° frames, with varied exposure times (10−30 s per frame) depending on the strength of diffraction. Empirical absorption corrections were applied to all data using SADABS.[25] The structures were solved with SHELXS-97[26] and refined with SHELXL-97[26] from data reduced with SAINT+ v. 6.02.[27] All solvent-accessible (VOID) volumes, pore electron populations (SQUEEZE), and residual electron density difference maps reported were calculated within PLATON.[28] Structure factor files (.fcf) incorporating any disorder were used when calculating solvent accessible volumes and pore electron populations. Guest atoms were eliminated for pore electron population and electron density difference map calculations. Channel and pore dimensions were calculated following subtraction of the relevant atomic van der Waals radii. Illustrations were produced using the programs WebLab ViewerPro[29] and ORTEP-3.[30] Full crystallographic tables, crystallographic information files (.cif), and ORTEP diagrams for all structures are provided in the Supporting Information. Details of the crystallographic modeling of disordered framework components and guest molecules are also included in the Supporting Information.

Single-Crystal X-ray Diffraction − Variable Temperature Unit Cell Determinations. Variable temperature unit cell determinations were carried out during the temperature ramping profiles outlined above. Multiple matrix collections (typically 45 0.3° frames) were performed automatically using *slam*-style command files within the SMART interface.[27] The temperature was ramped continuously over the appropriate ranges at rates between 10 and 20 K·h^{-1}. Unit cell data for the sorption of dichloromethane were not initially collected during cooling between 340 and 300 K due to an instrumental error; however, these data were later obtained by reheating the crystal in its sealed capillary through the temperature range.

Results

Thermogravimetry. TGA was used to investigate the desolvation and thermal decomposition of **1·(EtOH)**. As was observed for the nickel(II) analogue,[21] complete and rapid desolvation occurs with heating to 380 K as the ethanol is desorbed from the pores. The observed mass loss associated with this step of approximately 10% is consistent with the calculated value of 9.9% for one ethanol molecule per cobalt(II) atom. Beyond 380 K the now empty framework material, $Co(bpy)_{1.5}(NO_3)_2$ (**1**), is stable to 490 K where it begins to thermally decompose. TGA was further employed to monitor the sorption of potential guest molecules into the empty host framework **1**. Crystals of **1·(EtOH)** were heated to 393 K under a dry dinitrogen

(23) Fletcher, A. J.; Cussen, E. J.; Bradshaw, D.; Rosseinsky, M. J.; Thomas, K. M. *J. Am. Chem. Soc.* **2004**, *126*, 9750−9759.
(24) Cussen, E. J.; Claridge, J. B.; Rosseinsky, M. J.; Kepert, C. J. *J. Am. Chem. Soc.* **2002**, *124*, 9574−9581.
(25) Sheldrick, G. M. *SADABS, Empirical adsorption correction program for area detector data*; University of Göttingen: Göttingen, Germany, 1996.
(26) Sheldrick, G. M. *SHELXS-97, Program for crystal structure solution*; University of Göttingen: Göttingen, Germany, 1997.
(27) *SMART*, *SAINT*, and *XPREP*. *Area detector control and data integration and reduction software*; Bruker Analytical X-ray Instruments Inc.: Madison, WI, 1995.
(28) Spek, A. L. *Acta Crystallogr.* **1990**, *A46*, C43.
(29) *WebLab ViewerPro*, v. 3.7; Molecular Simulations Inc.: San Diego, CA, 2000.
(30) Farrugia, L. J. *J. Appl. Crystallogr.* **1997**, *30*, 565.

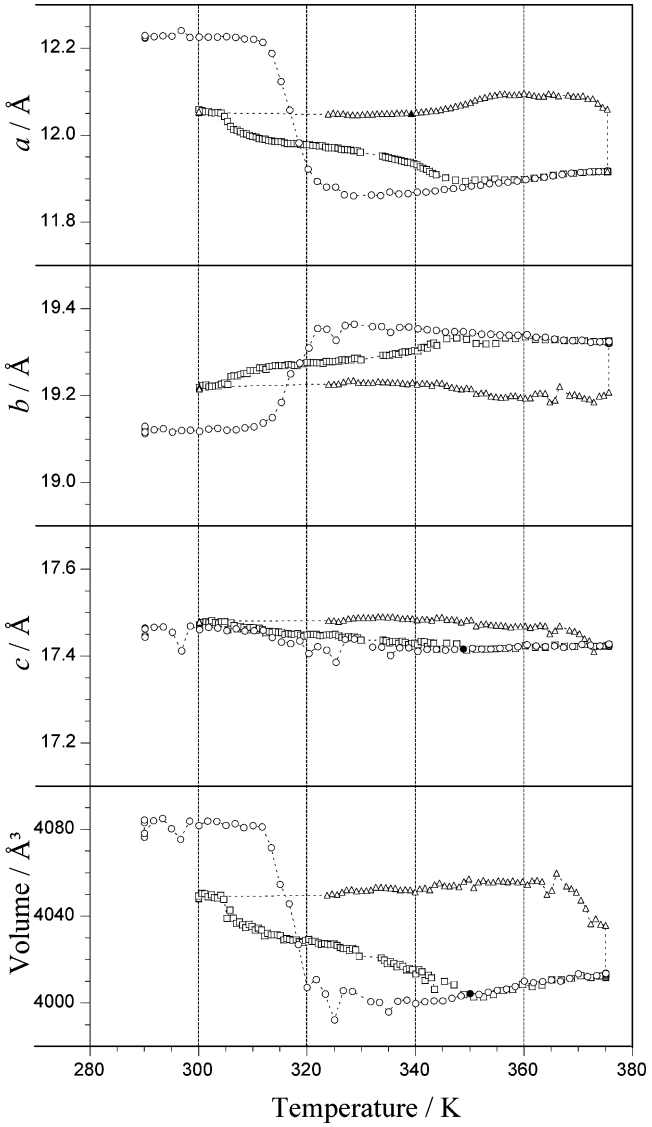

Figure 2. Evolution of the orthorhombic unit cell parameters and volume during the desorption process **1·(EtOH)** → **1** (○), the sorption process **1** → **1·(MeOH)** (△), and the desorption process **1·(MeOH)** → **1** (□), as measured by single-crystal X-ray diffraction.

atmosphere to give **1**, before being cooled to 298 K in the presence of the desired guest vapor. TGA data for the sorption of methanol (MeOH), acetone (ACN), acetonitrile (MeCN), tetrahydrofuran (THF), and dichloromethane (DCM) are included in the Supporting Information. A similar setup had been used previously to monitor the resolvation of the nickel(II) analogue with ethanol.[21] Here the sorption of all potential guests was observed, with approximate mass uptakes ranging from ∼3% for methanol to ∼6% for acetone. The extent of sorption for each guest depends on their individual vapor pressures and cannot be compared quantitatively. The observation of mass uptake for all five potential guests deemed them suitable for investigation by single-crystal X-ray diffraction.

Variable Temperature Unit Cell Determinations. Variable temperature unit cell determinations were employed to monitor the sorption and desorption of each of the guest species. Each sorption measurement was carried out on a fresh crystal and began with the desorption of ethanol from the as-grown material, **1·(EtOH)**, to give the empty host material, **1**. Figure 2 shows the evolution of the unit cell for the desorption process **1·(EtOH)** → **1**. The *a* and *b* parameters showed an abrupt change above 310 K, decreasing by 2.88(2)% and increasing by 1.14(3)%, respectively. The *c* parameter was essentially unaffected by the change in temperature, decreasing by ca. 0.2%. Overall, the unit cell volume decreased by 2.10(5)%, which is comparable to the 2.4% decrease observed for the nickel(II) analogue.[21] The steady, but less significant, increase of the *a* parameter and decrease of the *b* parameter above 335 K can be attributed to anisotropic thermal expansion following complete guest desorption. The opposing changes of the *a* and *b* parameters are the result of a scissoring action of the bilayers. Subsequent qualitative measurements found this process to be dependent on crystal size; larger crystals showed a more gradual decrease in unit cell volume, indicating that the desorption of ethanol occurs under kinetic control. Complete desorption of ethanol was assumed with a stable orthorhombic unit cell of approximately $a = 11.90$ Å, $b = 19.30$ Å, and $c = 17.45$ Å, with a volume of 4010−4020 Å^3.

The evolution of the unit cell for the sorption, and subsequent desorption, of methanol is shown in Figure 2. Dramatic changes in the unit cell parameters were observed immediately after exposure to methanol vapor. The *a* parameter increased to a maximum of 12.091(2) Å at 366 K, an increase of 1.46(2)%. Below this temperature, a gradual decrease in the *a* parameter persists that is consistent with anisotropic thermal contraction. Conversely, the *b* parameter exhibited a 0.64(4)% decrease during the sorption of methanol. A small, gradual increase in the *c* parameter (0.38(3)%) was observed as the exposed crystal was cooled. Overall, the unit cell volume behaved very similarly to the *a* parameter, with a total increase of 1.15(5)%. Notably, no framework transformation to the "ladder" phase was observed, as has been seen for methanol sorption into the Ni(II) analogue of this bilayer phase.[24] Following a full structural refinement of **1·(MeOH)**, the variable temperature unit cell was measured, as the material was again desolvated. The gradual desorption of the guest molecules was apparent as the unit cell parameters relaxed to the values previously observed for the fully desolvated phase, **1**. The desolvation process was complete by approximately 350 K, with the two cell evolutions merging above this temperature indicating the full reversibility of methanol sorption and desorption.

The sorption of acetonitrile, acetone, tetrahydrofuran, and dichloromethane is illustrated in Figure 3 as a function of the bilayer torsion angle, θ (the desorption of tetrahydrofuran is also included). θ is calculated directly from the unit cell parameters [$\theta = 2(\arctan(a/b))$] and indicates the degree to which the bilayer opens to accommodate the various guest species (Figure 1b). Full unit cell evolutions and descriptions are included in the Supporting Information. Significant increases in θ were apparent immediately after exposure to each of the guest vapors. For acetonitrile, dichloromethane, and acetone, θ rapidly reached maxima at 375 K of 65.2°, 67.4°, and 67.6°, respectively. Below this temperature, anisotropic thermal contraction results in a gradual decrease in θ, reaching respective minima of 64.1° (300 K), 65.7° (300 K), and 67.2° (320 K). For tetrahydrofuran, θ underwent an initial increase from 63.4° to 66.4° at 375 K and continued to gradually increase on cooling as more tetrahydrofuran was sorbed into the material, reaching a maximum of 68.7° at 310 K. Following a full structural

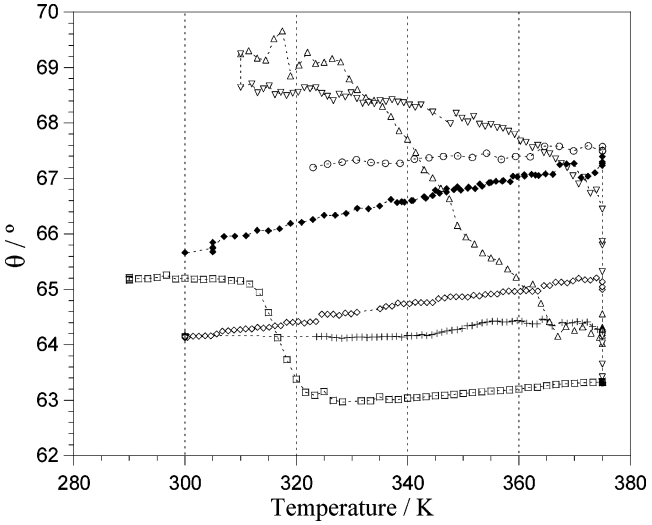

Figure 3. Evolution of the bilayer torsion angle (θ) on cooling during the processes **1 → 1·(MeCN)** (◇), **1 → 1·(DCM)** (◆), **1 → 1·(ACN)** (○), **1 → 1·(THF)** (▽), and **1·(THF) → 1** (△), as measured by single-crystal X-ray diffraction. The processes **1·(EtOH) → 1** (□) and **1 → 1·(MeOH)** (+) are also included.

refinement of **1·(THF)** there was a small increase in θ to 69.3°, indicating a small amount of further sorption. On heating, θ steadily relaxed to 64.0° at 375 K as tetrahydrofuran was liberated from the pores to again give the empty host **1**.

Analysis of the Bragg peak profiles revealed that no increase in crystal mosaicity occurred following the desorption and resorption processes, with peak rocking curves spanning ca. 0.4−0.5° in Ω (HWHM; cf. estimated instrument width of ca. 0.25° in Ω). Further, no structured diffuse scattering, superstructure reflections, or systematic absence violations were observed in any of the diffraction images for the partially sorbed phases, suggesting that no short- or long-range ordering of guests occurs in the one-dimensional pores.

Structural Characterizations. Structural characterizations were completed for the as-grown material (**1·(EtOH)**), the fully desorbed material (**1**), and each of the five sorbed materials (**1·(MeOH)**, **1·(MeCN)**, **1·(ACN)**, **1·(THF)**, and **1·(DCM)**). Summaries of crystallographic data are given in Table 1. Full data sets were collected, reduced, and refined to give near isostructural solutions to the nickel(II) analogue[21] and also the CS_2 and H_2O solvates previously reported for cobalt(II).[12,31] The basic building block of T-shaped coordination of three bpy molecules about the cobalt(II) atom was preserved, with two bidentate nitrate anions completing the coordination sphere. With the exception of **1·(DCM)**, the structural refinements of the materials were completed in the orthorhombic space group *Ccca* where the asymmetric unit consists of one-half of a cobalt(II), one-half of a "linear" bpy and one-fourth of a "bridging" bpy, one bidentate nitrate, and one-half of a guest molecule.

Despite initially appearing to have remained orthorhombic upon sorption of dichloromethane, the structure of **1·(DCM)** could not be solved or refined in *Ccca* or any related orthorhombic subgroups of *Ccca*. Upon reducing the unit cell to the primitive parent setting, a full structural refinement was successfully completed in the monoclinic space group *P*2/*n*. In this setting, the unit cell volume is approximately halved due to removal of the *C*-centering, and the symmetry lowering leads to doubling of the number of atoms in the asymmetric unit. The subsequent refinement of the structure revealed that the general framework motif of interdigitated bilayers was retained. However, upon closer inspection of the structure it was apparent that the bilayers were no longer evenly spaced, with the sorption of dichloromethane triggering a translation by 0.49 Å of one interpenetrated network of bilayers with respect to the other. This remarkable structural change is discussed in more detail below.

Discussion

The above crystallographic results represent the first of their kind, yielding highly accurate information on the structural consequences of guest molecule desorption and resorption in a porous framework solid. We note that Newsam et al.[32] have postulated the use of in situ single-crystal diffraction for investigations of sorption and ion exchange in microporous solids, but, to date, single-crystal diffraction has been performed only at fixed temperature and composition following ex situ modification.[33] To our knowledge, efforts to monitor host structures continuously during the sorption process, and therefore address questions on the nature of structural intermediates, have relied solely on the powder diffraction technique.[34,35]

Our efforts to synthesize the resorbed phases of **1** directly from solution have yielded only frameworks with the ladder topology,[24,36] thus **1·(MeOH)**, **1·(ACN)**, **1·(MeCN)**, **1·(THF)**, and **1·(DCM)** likely represent metastable framework phases. In addition to revealing the interactions of each guest within the pore structure of the host framework, these experiments have also highlighted the flexible nature of the host. This flexibility arises from a number of sources: intrabilayer flexibility, interbilayer flexibility, bpy torsional flexibility, and in the case of **1·(DCM)**, framework−framework translation, as described below.

Electron Density Difference Maps. Electron density difference maps are two-dimensional slices of residual electron density through a chosen plane of a material. By removing any guest atoms from refinements, maps depicting the electronic composition of the pores can be obtained. Electron density difference maps for equivalent planes in **1** and the guest-loaded materials **1·(guest)** are illustrated in Figure 4. The plane chosen clearly depicts the one-dimensional channels running horizontally across the maps in a zigzag fashion (the $y = {}^1/_2$ plane for orthorhombic structures and the $x - z = 0$ plane for **1·(DCM)**). Regions of positive electron density are indicated by gray contour lines. The pores are not uniform and can be considered as a series of cavities joined together by smaller window regions

(31) Power, N. K.; Hennigar, T. L.; Zaworotko, M. J. *New J. Chem.* **1998**, *22*, 177−181.

(32) Newsam, J. M.; Yang, C. Z.; King, H. E.; Jones, R. H.; Xie, D. *J. Phys. Chem. Solids* **1991**, *52*, 1281−1288.

(33) (a) Bae, D.; Seff, K. *Microporous Mesoporous Mater.* **2000**, *40*, 219−232. (b) Zhu, L.; Seff, K. *J. Phys. Chem. B* **2000**, *104*, 8946−8951. (c) van Koningsveld, H.; Jansen, J. C. *Microporous Mater.* **1996**, *6*, 159−167. (d) Ciraolo, M. F.; Hanson, J. C.; Toby, B. H.; Grey, C. P. *J. Phys. Chem. B* **2001**, *105*, 12330−12337. (e) Burzlaff, N. I.; Rutledge, P. J.; Clifton, I. J.; Hensgens, C. M. H.; Pickford, M.; Adlington, R. M.; Roach, P. L.; Baldwin, J. E. *Nature* **1999**, *401*, 721−724.

(34) Ciraolo, M. F.; Hanson, J. C.; Norby, P.; Grey, C. P. *J. Phys. Chem. B* **2001**, *105*, 2604−2611.

(35) (a) Lee, Y.; Reisner, B. A.; Hanson, J. C.; Jones, G. A.; Parise, J. B.; Corbin, D. R.; Toby, B. H.; Freitag, A.; Larese, J. Z. *J. Phys. Chem. B* **2001**, *105*, 7188−7199. (b) Nenoff, T. M.; Parise, J. B.; Jones, G. A.; Galya, L. G.; Corbin, D. R.; Stucky, G. D. *J. Phys. Chem.* **1996**, *100*, 14256−14264.

(36) Kepert, C. J.; Bevitt, J. J. University of Sydney, Australia. Unpublished results, 2002.

Table 1. Summary of the Single-Crystal X-ray Structural Data Collection and Refinement Data

compound	**1·(EtOH)**	**1**	**1·(MeCN)**	**1·(MeOH)**	**1·(DCM)**	**1·(ACN)**	**1·(THF)**
θ/deg	65.1	63.3	63.9	64.2	65.7	66.9	69.0
formula	$CoC_{15}H_{12}N_5O_6 \cdot C_2H_6O$	$CoC_{15}H_{12}N_5O_6$	$CoC_{15}H_{12}N_5O_6 \cdot C_2H_3N$	$CoC_{15}H_{12}N_5O_6 \cdot CH_4O$	$CoC_{15}H_{12}N_5O_6 \cdot CH_2Cl_2$	$CoC_{15}H_{12}N_5O_6 \cdot C_3H_6O$	$CoC_{15}H_{12}N_5O_6 \cdot C_4H_8O$
FW/g·mol^{-1}	463.29	417.23	458.28	449.27	502.15	475.30	489.33
T/K	293(2)	375(2)	300(2)	300(2)	305(2)	320(2)	310(2)
space group	*Ccca*	*Ccca*	*Ccca*	*Ccca*	*P*2/*n*	*Ccca*	*Ccca*
a/Å	12.220(4)	11.905(2)	11.984(2)	12.053(2)	11.3720(16)	12.699(13)	13.116(5)
b/Å	19.151(7)	19.325(3)	19.230(13)	19.227(2)	17.486(3)	19.21(2)	19.085(7)
c/Å	17.460(6)	17.425(3)	17.372(12)	17.480(2)	11.3736(16)	17.76(2)	17.934(7)
β/deg	90	90	90	90	114.319(2)	90	90
V/Å^3	4086(3)	4009.1(12)	4003(5)	4050.7(9)	2060.9(5)	4333(9)	4489(3)
Z	8	8	8	8	4	8	8
ρ_{calcd}/Mgm^{-3}	1.506	1.383	1.521	1.473	1.618	1.457	1.448
μ/mm^{-1}	0.889	0.895	0.905	0.895	1.136	0.841	0.814
data	2448	2363	2384	2335	4826	2350	2594
restraints	7	6	10	8	6	0	4
parameters	143	128	132	143	275	140	132
R(*F*) ($I > 2\sigma I$)	0.0444	0.0448	0.0714	0.0560	0.0455	0.0683	0.0944
R(*F*) (all data)	0.0562	0.0521	0.0841	0.0752	0.0505	0.0943	0.1295
$R_w(F^2)$ ($I > 2\sigma I$)	0.1277	0.1212	0.1899	0.1526	0.1236	0.1709	0.2571
$R_w(F^2)$ (all data)	0.1391	0.1287	0.1996	0.1707	0.1290	0.1945	0.2962
GOF	1.062	1.046	1.104	1.053	1.080	1.093	1.076
void volume/%	21.4	21.0	23.9	25.2	21.7	22.3	27.9
window size/Å^2	2.9 × 2.4	2.9 × 2.4	2.4 × 1.7	2.9 × 2.5	2.4 × 2.3	3.1 × 2.4	3.2 × 2.0
cavity size/Å^2	5.7 × 4.5	5.7 × 4.1	5.3 × 4.3	5.7 × 4.3	4.6 × 4.3	6.0 × 4.8	6.1 × 4.6
e$^-$/cavity (exptl)	26.3	1.1	23.9	21.1	44.3	22.1	37.5
e$^-$/cavity (expected)	26	0	22	18	42	32	36
			Interbilayer Hydrogen Bonds and Distances				
C1···O2′/Å	3.531(4)	3.444(4)	3.434(6)	3.484(5)	3.479(5) 3.521(5)	3.633(7)	3.841(9)
C2···O3′/Å	3.505(4)	3.479(4)	3.470(8) 3.448(11)	3.496(6)	3.441(5) 3.586(6)	3.632(8)	3.66(2) 3.902(14)
Co···Co′/Å	6.101(2)	6.0387(13)	6.017(5)	6.1008(15)	6.0583(11)	6.224(8)	6.382(3)
			Torsion Angles of bpy Ligands				
Ts (linear bpy)/deg	37.9(6)	29.2(7)	32.2(11)	31.3(9)	46.1(9) 22.0(13)	43.5(11)	45.9(15)
Ts (bridging bpy)/deg	33.2(3)	38.3(4)	34.4(7)	37.4(5)	31.5(3)	24.5(6)	21.6(7)
Ts (bpy−Co−bpy)/deg	37.7(4)	27.6(5)	32.1(7)	31.2(7)	45.3(6) 21.9(7)	39.7(7)	49.2(10)

to form one-dimensional channels (cavity and window dimensions are given in Table 1). For the as-grown ethanol-loaded material, **1·(EtOH)**, the residual electron density is concentrated at specific regions along the pores corresponding to the larger cavity regions. However, in the methanol-loaded material, **1·(MeOH)**, the smaller guest is distributed over a larger region of the pore, as illustrated by the almost continuous electron density along the channel. The near-linear acetonitrile guest molecule of **1·(MeCN)** is also able to accommodate both regions of the channel, but the majority of the electron density is located in the cavity region. For the larger guest molecules, acetone (**1·(ACN)**) and tetrahydrofuran (**1·(THF)**), the electron density is again concentrated in the cavity regions of the channels. The difference map for the dichloromethane-loaded material, **1·(DCM)**, indicates considerable residual electron density, as was expected given the large mass of the guest.

Guest Refinement. The guest molecule of each structure was located and carefully modeled for each refinement. The location of the guest molecules in each of the structural refinements is illustrated in Figure 5. A superimposed view of the local pore environment before and after guest sorption is given in Figure 6. All of the guests interact with the framework through hydrogen bonding interactions. Guest orientation in **1·(EtOH)** and **1·(MeOH)** is influenced by strong attractive hydrogen bonding interactions; both have four possible guest orientations within the pore, thereby interacting with the four unbound nitrate oxygen atoms that line each cavity region. For the weaker hydrogen bonding systems, **1·(ACN)**, **1·(MeCN)**, and **1·(THF)**, the guest orientation appears to be more influenced by repulsion; the acetone, acetonitrile, and tetrahydrofuran guests each exhibit two possible orientations arising from the C_2 symmetry in the pore. The reduction in symmetry from *Ccca* to *P*2/*n* observed for **1·(DCM)** eliminates the C_2 symmetry of the pore; here the dichloromethane molecule exhibits twofold positional disorder over two inequivalent sites.

Intrabilayer Flexibility. The two-dimensional bilayers that constitute the structures can be considered a kind of molecular "garden trellis". They are capable of opening and closing to some extent to accommodate guests of different size and shape. Figure 1c illustrates this action and defines the bilayer torsion angle, θ. The angle θ may be calculated directly from the unit cell parameters: for the orthorhombic phases $\theta = 2(\arctan(a/b))$ and for the monoclinic phase, **1·(DCM)**, $\theta = 180 - \beta$. In general, the bilayer torsion angle can be seen to increase as the size of the guest increases, from 63.3° for the empty host framework to a maximum of 69.0° for the tetrahydrofuran-loaded material. This action is the primary source of structural flexibility in the material, and the bilayer torsion angles provide a useful representative ordering for evaluating other trends. Interestingly, the linear acetonitrile molecule gives the most acute torsion angle of the guest-loaded frameworks. The smaller than perhaps expected torsion angle for **1·(DCM)** is likely related to the more complex framework translation associated with the sorption of dichloromethane.

Interbilayer Flexibility. Flexibility was also observed between the bilayers. Alternate bilayers interact through mul-

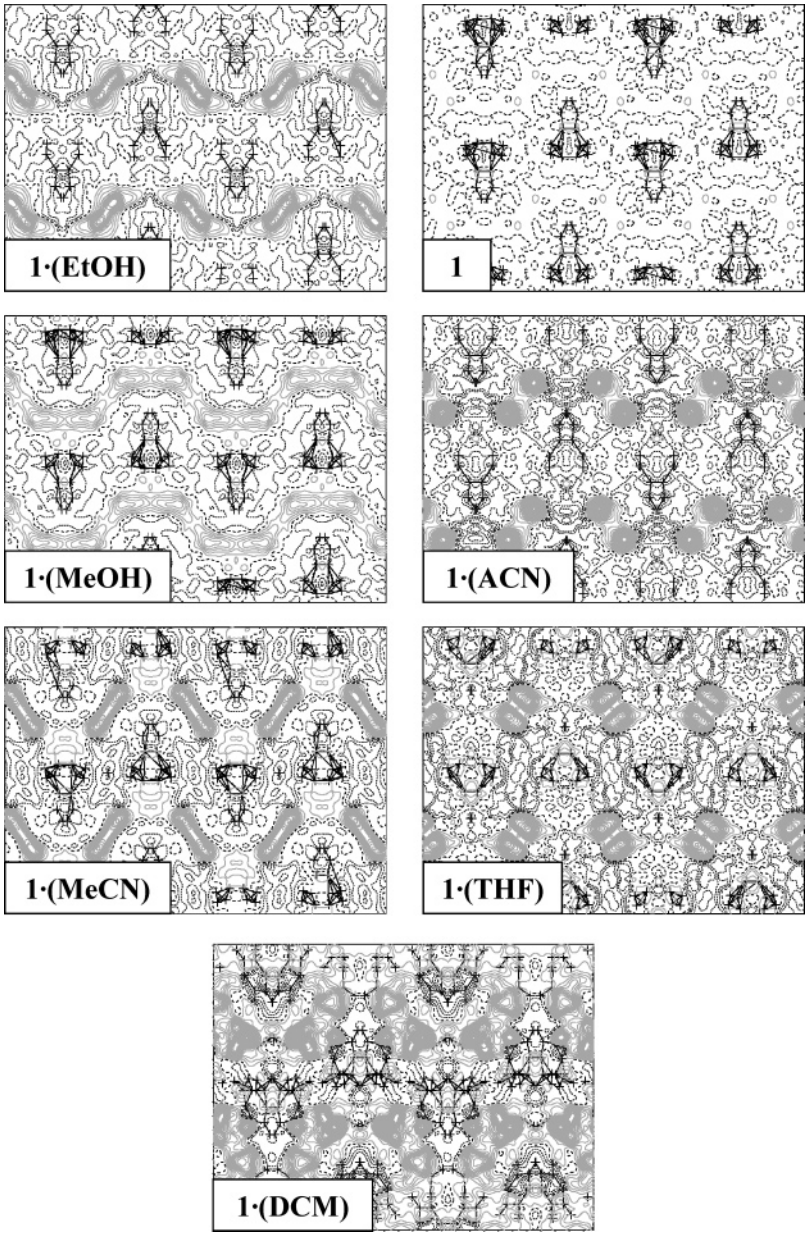

Figure 4. Electron density difference maps illustrating the electron population of the zigzag 1-D pores. The horizontal axis, corresponding to the pore direction, is [100] in all cases except the lower symmetry phase, **1·(DCM)**, where this is the [110] direction. The vertical axis corresponds to the [001] direction in all cases. Gray contours indicate regions of positive electron density.

tiple hydrogen bonds, thereby extending the two-dimensional bilayers into essentially a doubly interpenetrated three-dimensional network. The hydrogen bond distances and also the cobalt···cobalt separations across them are tabulated for each of the structural refinements in Table 1. There is a general increase in each of the distances with increasing bilayer torsion angle, with the exception of **1·(DCM)**. The hydrogen bonds and cobalt···cobalt separations are of comparable length for the empty host framework and when loaded with ethanol, methanol, acetonitrile, and dichloromethane (hydrogen bonds: ∼3.43−3.55 Å, Co···Co: ∼6.04−6.10 Å). In accommodating acetone and tetrahydrofuran, the interlayer hydrogen bonding interactions lengthen to donor−acceptor distances ranging from ∼3.6−3.9 Å. Concomitant increases in the cobalt···cobalt separations to 6.224(8) Å for acetone and 6.382(3) Å for tetrahydrofuran were observed. These increases in distance suggest that sorption of acetone and tetrahydrofuran may considerably weaken the interbilayer hydrogen bonding. In contrast, it seems likely that a major driving force for the framework translation in **1·(DCM)** is the retention of the interbilayer hydrogen bonding interactions.

Framework Translation in 1·(DCM). The interpenetrating networks are equally spaced in all structures excluding the dichloromethane-loaded material **1·(DCM)**. Upon sorption of dichloromethane there is a shift of one interpenetrated net with respect to the other by a distance of 0.49 Å. This translation is evident in Figures 5 and 6 and is illustrated schematically in Figure 7. The resulting uneven spacing of the bilayers is reflected in the decrease in symmetry from *Ccca* to *P*2/*n*. Only very weak van der Waals interactions are present between the two interpenetrating networks for both the equally spaced and translated structures, and therefore it is expected that the network translation occurs via a very low energy pathway.

Analysis of intermolecular host−guest distances for **1·(EtOH)**, **1·(MeCN)**, **1·(MeOH)**, **1·(ACN)**, and **1·(THF)**

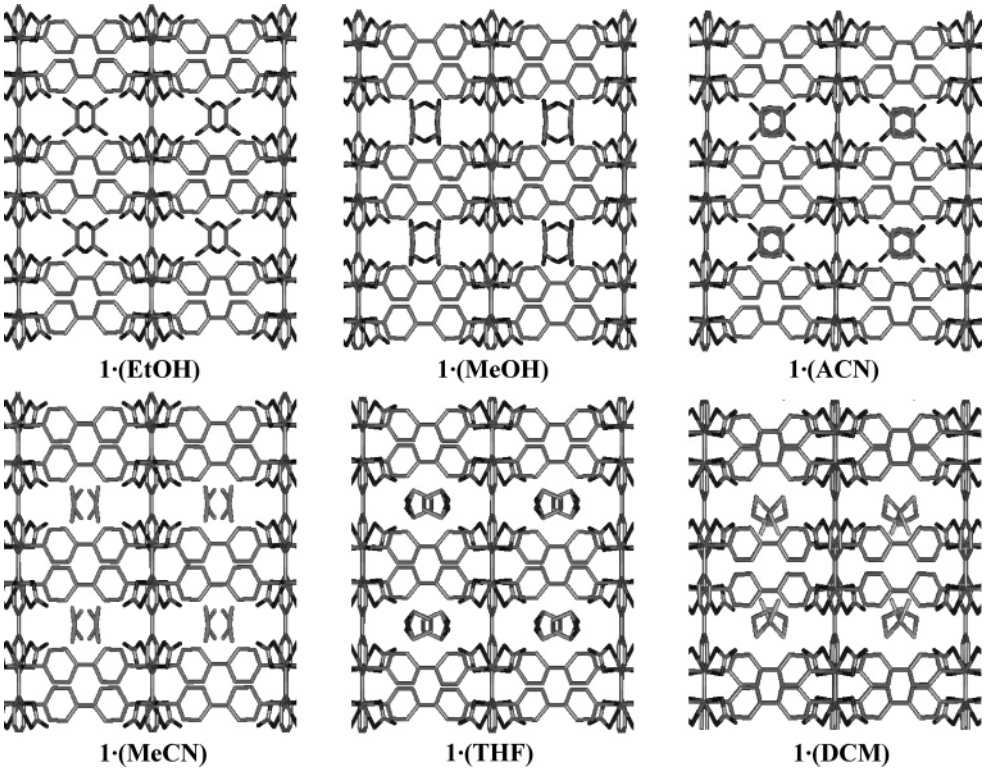

Figure 5. Stick representation indicating the guest location in the crystal structures of **1·(guest)**. Views are given directly down the 1-D channel axis, corresponding to the [100] direction in **1·(EtOH)**, **1·(MeOH)**, **1·(ACN)**, **1·(MeCN)**, and **1·(THF)**, and the [110] direction in **1·(DCM)**. The [001] direction is aligned vertically in all cases. Hydrogen atoms and framework disorder have been omitted for clarity.

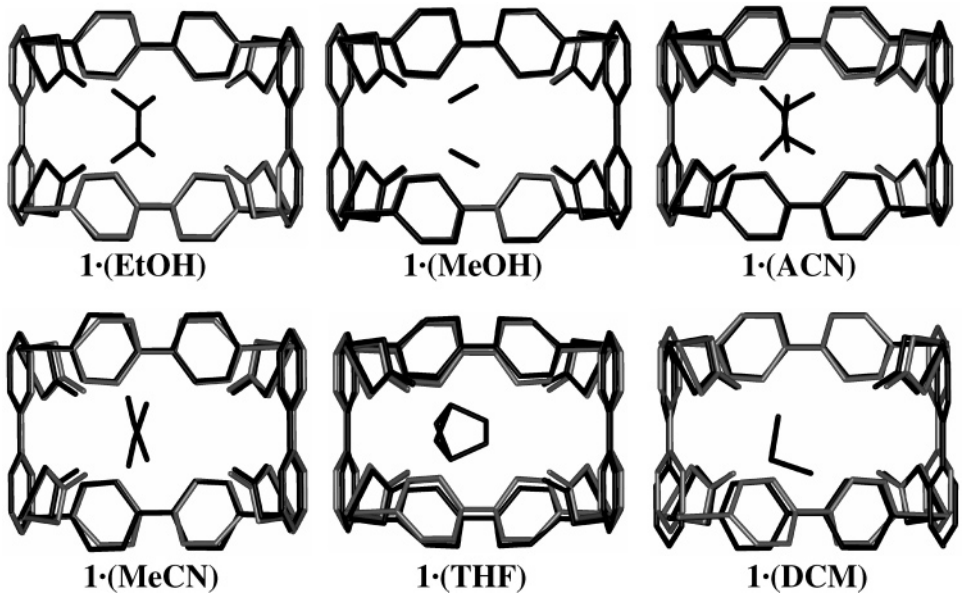

Figure 6. Superimposed local pore environments for each of the guest-loaded phases (black) with the fully desorbed phase (gray). Nitrate disorder and hydrogen atoms have been omitted for clarity.

reveals that all significant host−guest interactions occur locally with only one of the two interpenetrating nets (i.e., for these guests the local pore environment is defined by a single net). For the dichloromethane guest, however, the second interpenetrated net becomes available to participate in long-distance C−Cl···H−C hydrogen bonding interactions.[37] In the translated structure of **1·(DCM)** there are two inequivalent, disordered orientations of the dichloromethane guest. Both of these orientations form C−Cl···H−C hydrogen bonds with each of the interpenetrated networks (see Figure 8 and Table 2). Notably, atom Cl1, which is approximately superimposed for the two guest orientations and was modeled as a single atom site, forms hydrogen bonds to both C12 on the nearest net and to the hydrogen atoms of C4 and C5 of the alternate net. Similarly, atom Cl2A forms hydrogen bonds to each of the interpenetrated nets. In comparison, the similar location of the dichloromethane guest in the equally spaced interpenetrated host lattice led to chemically unreasonable hydrogen bonding distances.

(37) Aakeröy, C. B.; Evans, T. A.; Seddon, K. R.; Palinko, I. *New J. Chem.* **1999**, *23*, 145−152.

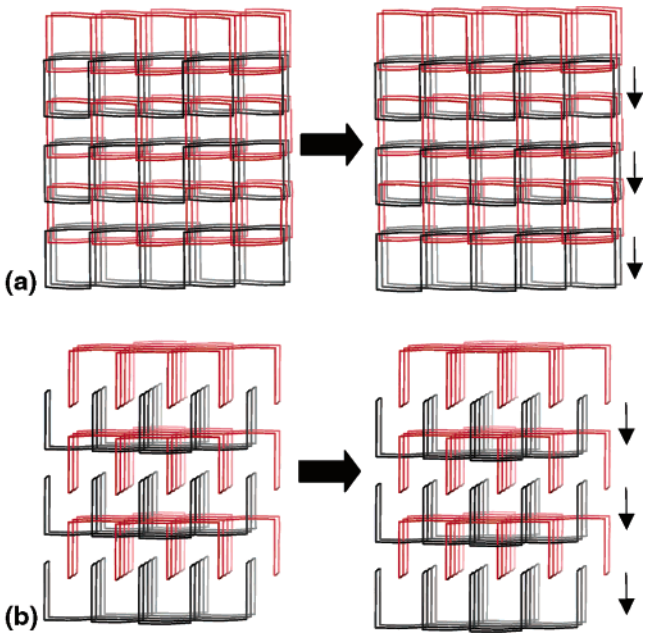

Figure 7. Diagrammatic representation of the bilayer translation observed in **1·(DCM)** as viewed along the (a) [100] and (b) [110] directions of the parent orthorhombic cell, showing the downward displacement of the black net with respect to the red net.

Torsion Angles of bpy Ligands. There are three different bpy torsion angles defined by the structural motif, one for each of the two types of bpy ligands, Ts(linear bpy) and Ts(bridging bpy), and a third for the torsion angle of the "linear" bpy ligands across the cobalt atom, Ts(bpy−Co−bpy). In the larger asymmetric unit of **1·(DCM)** each of these splits into two inequivalent angles. These angles have been compiled in Table 1. There is considerable variation in each of the torsion angles across the different structures, further highlighting the remarkable structural flexibility of this phase. For both the "linear" bpy and the bpy−Co−bpy angles, there is generally an increase as the bilayer torsion angle increases. Conversely, for the "bridging" bpy the torsion angle decreases as the bilayer torsion angle increases. The only significant exception is the more complex behavior of **1·(DCM)**, where the "bridging" bpy remains essentially unchanged upon sorption and the two different angles across both the bpy−Co−bpy and the "linear" bpy have opposing behaviors.

Framework Disorder. In almost all of the structural refinements disorder was observed in the nitrates and/or the C4 and C5 atoms of the "linear" bpy. The minor monodentate disorder of the nitrate is prevalent only in the structural refinements where either no guest or a smaller guest is present (**1, 1·(EtOH)**, **1·(MeOH)**, **1·(MeCN)**). As the monodentate component projects into the cavity, the presence of a larger guest molecule may inhibit this disorder. The nitrate in **1·(MeCN)** is heavily disordered with three possible orientations featuring two possible unbound oxygen positions, both of which are involved in hydrogen bonding with the guest molecule. The unbound nitrate oxygen atom in **1·(THF)** is disordered over two possible sites, with the greater occupied B component forming significantly shorter (∼0.2 Å) hydrogen bonds with the guest tetrahydrofuran molecule. The C4 and C5 atoms of the "linear" bpy are ordered in only the as-grown material **1·(EtOH)** and in the acetone-loaded host **1·(ACN)**. These atoms are not involved in any hydrogen bonding interactions, unlike the atoms on the opposite side of the pyridyl unit, which are involved in the interbilayer hydrogen bonding (Figure 1a). There appears to be no direct correlation between ordering of the pyridyl units and strength of the interbilayer hydrogen bonding, since **1·(EtOH)** and **1·(ACN)** have mid-length hydrogen bonding interactions in comparison to the other materials.

Conclusions

Through modified single-crystal X-ray diffraction experiments the robust but subtly flexible coordination framework, **1·(guest)**, has been explored, yielding unique information on the structural consequences of reversible guest sorption in this phase. The use of a time-resolved, in situ single-crystal X-ray diffraction technique demonstrates that the sorption and desorption processes occur homogeneously within single crystals of this coordination framework host. The flexibility of the interpenetrated host structure results primarily from a "garden-trellis"-like action of the bilayers, allowing the framework to reversibly accommodate guests of different size and shape. For larger guests such as acetone and tetrahydrofuran, a slight lengthening of interbilayer hydrogen bonding interactions is evident; it is likely that the formation of favorable host−guest interactions compensates for the apparent weakening of these host−host hydrogen bonds. Upon sorption of dichloromethane, the material undergoes a remarkable framework−framework translation, resulting in a decrease from *C*-centered orthorhombic to primitive monoclinic symmetry. This translation occurs in preference to a further expansion of the interbilayer distance and appears to result directly from the ability of the dichloromethane molecule to form hydrogen bonds to each of the two interpenetrated networks. The sorption of each of the guests also had minor implications on the disordered components of the framework and the torsion angles of the bpy ligands, although no consistent trends emerged. The observation of considerable structural flexibility in this phase is consistent with previous reports of unusual sorption behavior for this phase, where it was proposed that host flexibility is driven by host−guest interactions.[13,23] We note that the subtle flexibility of **1·(guest)** is in stark contrast to the transformation reported for the nickel(II) analogue,[24] where the sorption of methanol vapor (over 24 h) caused a solid-state transformation to give a one-dimensional structural polymorph with the ladder topology.

The majority of coordination framework materials reported to date have been found to exhibit no significant structural changes during guest exchange.[5,9,16] In recent years, however, a number of interesting exceptions have arisen, highlighting the novel flexibility of molecular hosts and necessitating the development of new structural approaches to follow host lattice transformations: notably, Kitagawa and co-workers have recently used in situ synchrotron X-ray powder diffraction to characterize the shape-responsive fitting of a shrinkable framework host;[14] Fujita and co-workers have reported ex situ crystal-to-crystal sliding[19] and expansion/contraction[18] transformations in two separate coordination frameworks; and Suh and Choi have reported a crystal-to-crystal transformation following ex situ framework oxidation by iodine guests.[20] Also of interest has been the observation of guest-driven interconversion between different framework topologies, requiring breakage and formation of coordination bonds within the host lattice.[8,24]

The present investigation confirms that porous framework materials may remain monocrystalline throughout both the guest

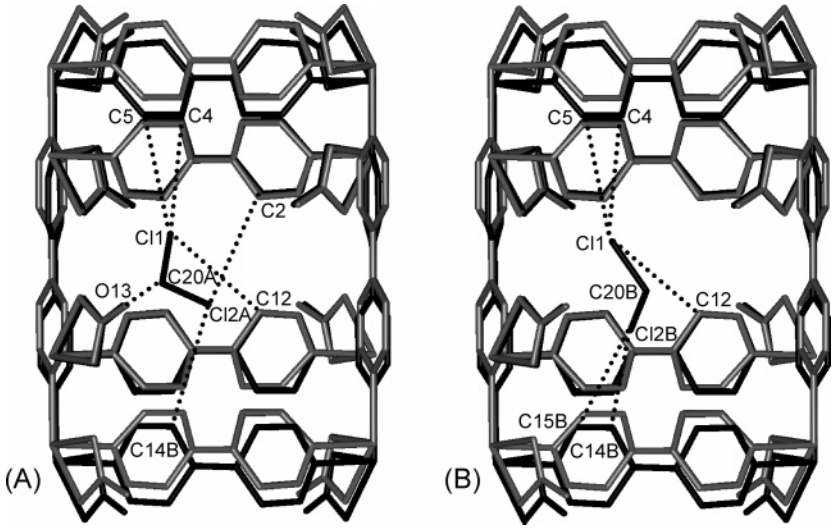

Figure 8. Hydrogen bonding interactions of the two disordered orientations (A and B) of the dichloromethane molecule within the interpenetrated bilayer framework structure of **1·(DCM)**. The existence of significant hydrogen bonding interactions to both of the interpenetrated bilayers (see Table 2) is unique for this guest and appears to be responsible for the bilayer translation; all other guests investigated interact locally with only one of the two bilayer nets. The superimposition of **1·(DCM)** (black) and the empty host **1** (gray) highlights the structural translation. Framework disorder and hydrogen atoms have been omitted for clarity.

Table 2. Host−Guest Hydrogen Bonding Interactions for **1·(DCM)**

D–H···A	D–H (Å)	H···A (Å)	D···A (Å)	D–H···A (deg)
C20A−H20B···O13[a]	0.97	2.38	3.220(18)	144
C4−H4···Cl1[b]	0.93	3.42	4.045(5)	127
C5−H5···Cl1[b]	0.93	3.30	3.995(5)	134
C12−H12···Cl1[c]	0.93	3.26	4.008(5)	139
C2−H2···Cl2A[d]	0.93	3.32	3.805(7)	115
C14B−H14B···Cl2A[b]	0.93	3.11	3.923(10)	147
C14B−H14B···Cl2B[b]	0.93	2.67	3.315(11)	127
C15B−H15B···Cl2B[b]	0.93	2.79	3.386(10)	123

[a] Symmetry code: $-x + 3/2, y, -z + 3/2$. [b] Symmetry code: $-x + 1, -y, -z + 1$. [c] Symmetry code: $-x + 1/2, y, -z + 1/2$. [d] Symmetry code: $x, y + 1, z$.

desorption and sorption processes and that no associated increase in crystal mosaicity occurs either during or after these processes. The use of a novel in situ X-ray diffraction technique, in which single crystals are monitored continuously during guest desorption and sorption, has shown also that there is no evidence for partial ordering of guests in the channels in the partially sorbed phases. The flexibility of **1·(guest)** is a property rarely observed in microporous hosts and arises here due to the energies of guest sorption apparently being comparable to those of the various framework distortions observed; such a feature is largely absent in other microporous phases such as the zeolite family, for which few instances of significant host flexibility are known.[35] This property has interesting implications to the potential application of coordination frameworks as selective hosts, since selectivity in the host−guest interaction within such hosts is influenced not just by conventional size and shape effects, but by the ability of the guest to participate in host−guest interactions of sufficient strength to favor distortion of the flexible framework lattice.

Acknowledgment. We thank the Australian Research Council for funding.

Supporting Information Available: Thermogravimetric data. Complete variable temperature unit cell plots. Details and figures for crystallographic modeling of disordered components. Crystallographic tables and CIF files. This material is available free of charge via the Internet at http://pubs.acs.org.

JA042420K